ADVANCED OPTICAL MATERIALS

www.advopticalmat.de

# Efficient Mid-Infrared Light Confinement within Sub-5-nm Gaps for Extreme Field Enhancement

*Dengxin Ji, Alec Cheney, Nan Zhang, Haomin Song, Jun Gao, Xie Zeng, Haifeng Hu, Suhua Jiang, Zongfu Yu, and Qiaoqiang Gan**

**Optical field can be concentrated into deep-subwavelength volumes and realize significant localized-field enhancement (so called "hot spot") using metallic nanostructures. It is generally believed that smaller gaps between metallic nanopatterns will result in stronger localized field due to optically driven free electrons coupled across the gap. However, it is challenging to squeeze light into extreme dimensions with high efficiencies mainly due to the conventional optical diffraction limit. Here a metamaterial super absorber structure is reported with sub-5 nm gaps fabricated using atomic layer deposition processes that can trap light efficiently within these extreme volumes. Light trapping efficiencies up to 81% are experimentally demonstrated at mid-infrared wavelengths. Importantly, the strong localized field supported in these nanogap super absorbing metamaterial patterns can significantly enhance light–matter interaction at the nanoscale, which will enable the development of novel on-chip energy harvesting/conversion, and surface enhanced spectroscopy techniques for bio/chemical sensing. By coating these structures with chemical/biological molecules, it is successfully demonstrated that the fingerprints of molecules in the mid-infrared absorption spectroscopy are enhanced significantly with the enhancement factor up to $10^6$–$10^7$, representing a record for surface enhanced infrared absorption spectroscopy.**

## 1. Introduction

Due to the diffraction limit of conventional optics, coupling and confinement of light into deep-subwavelength volume is usually very challenging, resulting in difficulties in exploring the light–matter interaction within these ultrathin (1D) or ultrasmall dimensions (2D or 3D). The unprecedented ability of metallic nanostructures with nanometric gaps to concentrate light has attracted significant research interest in recent years.[1,2] It has been reported that the optical field can be concentrated into deep-subwavelength volumes and realize significant localized-field enhancement using a variety of nanoantenna structures,[3] showing promise for the development of enhanced nonlinear optics,[4] surface photocatalysis,[5,6] and vibrational biosensing spectroscopies.[7,8] It is generally believed that smaller gaps between metallic nanopatterns will result in stronger localized-field enhancement due to optically driven free electrons coupled across the gap. According to previous research, visible light can be squeezed into a 3 nm metal–insulator–metal plasmonic cavity with both open[9] and closed ends.[10] In other recent work, an electric field enhancement of 1000 was experimentally demonstrated for a nonresonant 70 nm wide slit in the terahertz regime.[11] Following the prediction that the field enhancement will keep increasing with decreasing gap size, much larger enhancement (e.g., 25 000) was observed for a 1 nm gap at the wavelength of ≈4 mm.[12] This increasing enhancement continues until the gap is scaled down into quantum regimes (i.e., 0.3–0.5 nm), where the upper limit for plasmonic field enhancement can be obtained.[13–17] Therefore, structures with extremely small gap features are highly desired for light–matter interaction applications based on maximized field confinement and enhancement. However, it is challenging to fabricate nanophotonic structures with such small features to squeeze light into these extreme dimensions efficiently.

Atomic layer lithography pioneered by refs. [12] and [18–23] is a new technology to fabricate deep-subwavelength uniform features. In this manufacturing process, atomic layer deposition (ALD) is used to define nanogaps between predefined nanopatterns and deposited metal films, giving Angstrom-scale lateral resolution along the entire contour of structures. In the originally proposed strategy,[12] the upper metal patterns have to be peeled off using standard adhesive tape, which is a critical step of this ALD lithography process. To realize the final metal patterns with very small gaps, it is crucial to fabricate

D. Ji, A. Cheney, N. Zhang, H. Song, Dr. X. Zeng, Prof. Q. Gan
Department of Electrical Engineering
The State University of New York at Buffalo
Buffalo, NY 14260, USA
E-mail: qqgan@buffalo.edu
J. Gao, Prof. S. Jiang
Material Science Department
Fudan University
Shanghai 200433, China
Prof. H. Hu
College of Information Science and Engineering
Northeastern University
Shenyang 110819, China
Prof. Z. Yu
Department of Electrical and Computer Engineering
University of Wisconsin
Madison, WI 53705, USA

**DOI: 10.1002/adom.201700223**

 

vertical sidewalls on the first layer, so that there is a discontinuity between the first layer and the second, as reported in refs. [12,18], and [19]. Nevertheless, it is challenging to control the sidewall verticality of the first metal layer and thickness of the second metal film to obtain the tiny discontinuity. If the second layer is thick and forms a continuous film, the entire layer will be peeled off. Recently, several groups including our own developed modified processes to avoid the challenging control of the side-wall and the second layer deposition.[20,24] Instead, the entire three-layered nanopattern (i.e., the first predesigned nanopattern, the second ALD layer, and the third metal deposition) is peeled from the substrate, demonstrating a strategy to develop nanopatterns with ALD-defined gaps over large areas that can increase the fabrication quality and yield.[24] However, although the localized field can be enhanced significantly within smaller gaps, the light coupling efficiency from free-space into these ultrasmall volumes is usually very weak due to the diffraction limit of conventional optics. For instance, the peak light coupling efficiency in periodic patterns with 3 nm gaps is only 3%.[20] Most incident energy was lost due to the weak coupling. Therefore, it is essential to develop new structures to improve the light trapping performance and further enhance the localized field in these extreme volumes.

It was recently recognized that patterned metamaterial super absorber structures provide a planar photonic platform to control the electromagnetic fields in ultrathin/small dimensions with flexibility and performance that was not previously possible.[25] A particularly exciting opportunity has emerged in thin-film metamaterial super absorbers capable of near-perfect light absorption.[26] These resonant on-chip structures provide a promising platform for the efficient coupling and concentration of incident light into subwavelength volumes. In this article, we will combine the super absorbing metamerial structure with modified ALD lithography to develop a super absorbing nanogap metamaterial with sub-5 nm gaps. By squeatezing mid-infrared (mid-IR) light into nanogaps efficiently, our structure can obtain extremely enhanced light fields that are particularly useful for enhanced light–matter interaction, as demostrated using surface enhanced infrared absorption (SEIRA) spectroscopy.

## 2. Interaction between Adjacent Patterns in Planar Metal–Dielectric–Metal (MDM) Structures

As illustrated in **Figure 1**a, a typical three-layered planar MDM metamaterial super absorber structure is constructed by a continuous metal ground plane, a dielectric spacer layer, and a top (periodic[26] or nonperiodic)[27,28] nanopattern array. According to the microscopic description of the physical operating mechanism,[11] when the distance between each nanopattern is sufficiently large, the interaction between adjacent nanopatterns is negligible, the three-layered unit can be treated as an optical analogue of a grounded patch antenna, with a fixed spectral resonance. The position of this absorption resonance is mainly determined by geometric parameters of an individual grounded

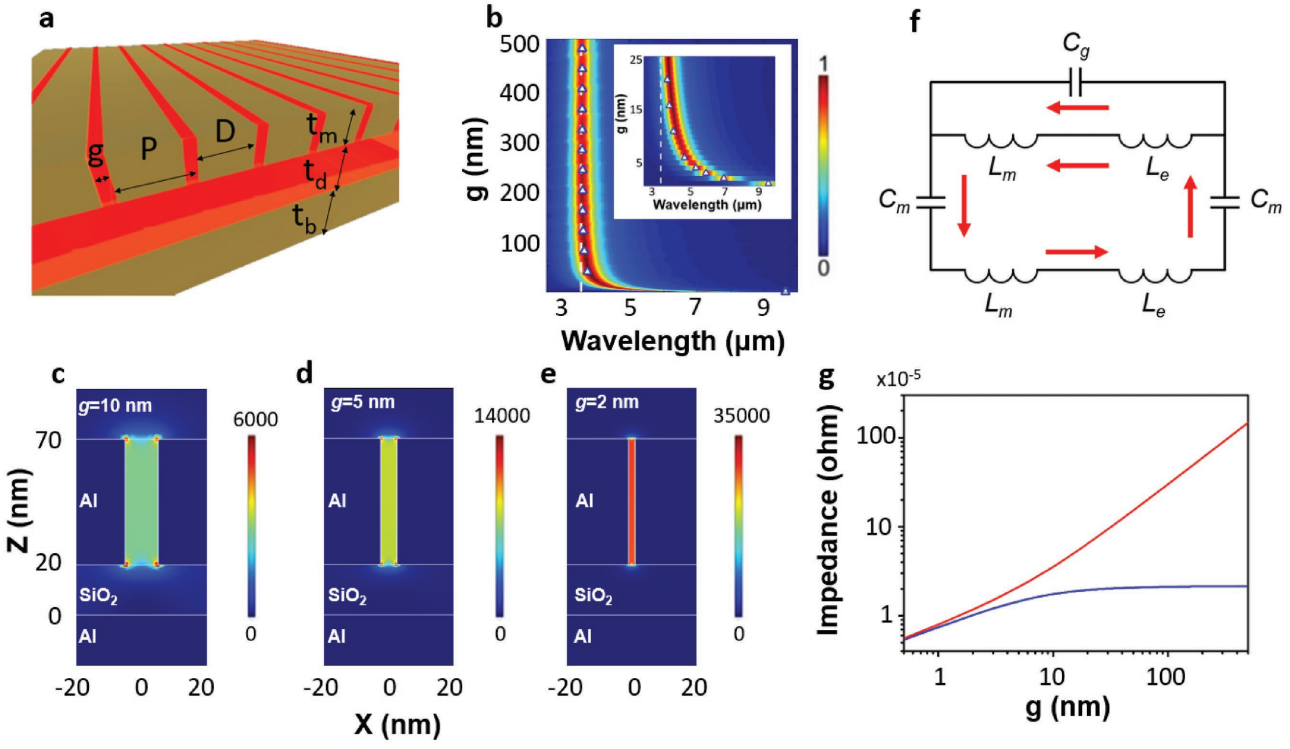


**Figure 1.** a) Conceptual illustration of metamaterial structure with 1D periodic distributed patterns on the top surface. b) Preliminary modeling of the absorption spectra of patterned MDM super absorber structures. Localized-field enhancement distribution (i.e., $|E/E_0|^2$) within the c) 10 nm wide, d) 5 nm wide, and e) 2 nm wide gaps. f) Effective circuit model for MDM super absorber structure. g) Impedances of $C_g$ (red curve) and ($L_m + L_e$) (blue curve) at different gap distance. The dashed line shows the impedance of ($L_m + L_e$) at resonant wavelength for a single grounded patch antenna.

patch antenna rather than the period.[28] However, when the gaps are reduced to sub-10 nm scales, adjacent modes will strongly interact with each other and result in extreme localized field with an absorption peak that also depends strongly on gap size.

To demonstrate this mechanism, we plot the absorption spectra of a 1D MDM metamaterial super absorber as the function of the gap distance, *g*. All other geometric parameters are fixed [i.e., the width ($D$), the thickness of the top pattern ($t_m$), the thickness of the spacer layer ($t_d$), and the thickness of the bottom layer ($t_b$) are fixed at 700, 50, 20, and 100 nm, respectively]. As shown in Figure 1b, one can see that the perfect absorption peak (close to 100%) is fixed in the range of 3.5–3.7 μm when the gap between ajacent patterns, *g*, is larger than 50 nm. However, in the small gap-distance region, the absorption resonance will significantly shift toward the long wavelength region due to the interaction between adjacent patterns (see the inset of Figure 1b). Specifically, when *g* is reduced to 10 nm, the perfect absorption resonance is tuned to 4.52 μm, with an enhancement factor (i.e., $|E/E_0|^2$) of >6000 (Figure 1c). If *g* is reduced to 5 nm, the perfect absorption is shifted to 5.29 μm and the localized enhancement factor is increased to >14 000, as shown in Figure 1d. If *g* is further reduced to 2 nm, the strong absorption (over 71%) is still realizable at 7.16 μm and the localized-field enhancement factor is enhanced to >35 000, as shown in Figure 1e. These modeling data indicate the potential to efficiently concentrate the light into extremely deep subwavelength volumes for enhanced light–matter interaction, which has not been realized by previously reported nanostructures.

To interpret the shifted resonance in mid-IR spectral region, here we employ the optical nanocircuit theorem[29–32] to analyze the resonance condition, as illustrated in Figure 1f. The resonance condition for the fundamental magnetic resonance mode can be obtained by canceling the total impedance[29]

$$Z_{tot}(\omega) = j\omega\cdot\left[\frac{L_m + L_e}{1-\omega^2 C_g(L_m+L_e)} - \frac{2}{\omega^2 C_m} + L_m + L_e\right] \quad (1)$$

Here $L_m = 0.5\,\mu_0 t_d D/l$ accounts for the parallel-plate inductance; $\mu_0$ is the vacuum permeability; $l$ is the length along the groove direction; $C_m = c_1\varepsilon_d\varepsilon_0 Dl/t_d$ represents the parallel-plate capacitance. Parallel-plate capacitance $C_g = c_2\varepsilon_g\varepsilon_0\, t_m l/g$ is used to describe the gap capacitance between neighboring patterns. Constants $c_1 = 0.21$ is related to the nonuniform charge distribution caused by magnetic resonance,[33] $c_2 = 2.4$ is the correction factor due to fringing effect of capacitance.[34] $\varepsilon_d$, $\varepsilon_g$, and $\varepsilon_0$ are the relative permittivities of dielectric spacer material, gap material, and the vacuum, respectively. A general form of kinetic inductance $L_e = -D/\left(\omega^2 t_{meff} l\varepsilon_0\varepsilon'_m\right)$ is employed by considering the real part of dielectric function ($\varepsilon'_m$) of Al. The effective thickness ($t_{meff}$) for electric currents is defined as the power penetration depth $\delta$ if $\delta < t_m$ ($\delta = \sqrt{\rho(\pi f\mu)}$, where $\rho$ is the resistivity of the conductor, $f$ is the frequency, $\mu$ is the absolute magnetic permeability of the conductor). Otherwise, $t_{meff} = t_m$. The resonant condition is mainly determined by $C_g$ and ($L_m + L_e$), simultaneously ($C_m$ is independent on *g*). To further reveal their respective contributions, the impedance values of $C_g$ and ($L_m + L_e$) at the resonant wavelength as the function of *g* are plotted in Figure 1g. When the gap size is sufficiently large, the absolute impedance of $C_g$ (red curve) is much larger than that of ($L_m + L_e$) (blue curve). Since $C_g$ and ($L_m + L_e$) are in parallel, the impedance induced by $C_g$ can be neglected, i.e., the resonant wavelength is insensitive to the gap distance, *g*, and only determined by the impedance of ($L_m + L_e$), which is almost a constant (see the dashed line in Figure 1g). In this case, the corresponding wavelength set the lower limit of the resonant wavelength for the MDM super absorber structure (see the white dashed line in Figure 1b). This is consistent with the previously reported conclusion:[28] i.e., when the distance between each nanopattern is so large that the interaction between adjacent nanopatterns is negligible, the resonant wavelength is mainly determined by the geometric parameters of the individual optical patch antenna.

On the other hand, as *g* decreases, $C_g$ becomes non-negligible. As shown in Figure 1g, the two curves for $C_g$ and ($L_m + L_e$) get close to each other and therefore determine the resonant wavelength of the circuit simultaneously. As shown by empty triangles in Figure 1b, the resonant wavelength for different gap distance is plotted using Equation (1), agreeing well with the numerical modeling (including the small *g* region, as shown in the inset of Figure 1b). Therefore, this nanogap MDM does provide a way to enhance the light–matter interaction within extremely small volumes that approach the theoretical upper limit[14] (it should be noted that the quantum limit identified by ref. [13] cannot be predicted accurately using this classical model). However, this planar MDM structure is extremely difficult to fabricate using the originally proposed ALD lithography process.[12] Instead, here we propose an alternative corrugated metamaterial structure to overcome those challenges in fabrication to realize the extremely enhanced field within extremely small gaps over large areas.

## 3. Efficient Light Trapping in Corrugated MDM Structure with ALD-Defined Gaps

The schematic diagram of the new structure is illustrated in **Figure 2**a. The ground plate is a corrugated grating with a top antenna pattern embedded in the trench of the grating and isolated by very narrow gaps. The top surface of the structure is flat. By selecting suitable parameters (e.g., $P$ = 600 nm, $D$ = 300 nm, $t_m$ = 40 nm, $t_d$ = 60 nm, $g$ = 5 nm, $t_b$ = 100 nm), a resonant perfect absorption at 5.54 μm can be obtained, as shown in Figure 2b. This resonant wavelength can also be explained using the optical nanocircuit theorem, as illustrated in Figure 2c. In this case, the resonant wavelength condition can be determined by zeroing the total impedance of this circuit

$$Z_{tot}(\omega) = j2\omega\left[\frac{-\frac{1}{\omega^2} + C_g\left(L'_m + L'_e\right)}{\left(C_m + C_g\right) - \omega^2 C_m C_g\left(L'_m + L'_e\right)} + \left(L_m + L_e\right)\right] \quad (2)$$

where $L'_m = 0.5\mu_0\left(D+2g\right)\left(t_m + t_d\right)/l$ is the mutual inductance caused by the parallel-plate inductance; $L'_e = -\left(t_m + t_d\right)/\left(\omega^2 t_{meff} l\varepsilon_0\varepsilon'_m\right)$ is the kinetic inductance of the side wall of the second metal layer. Using this equation, the resonant

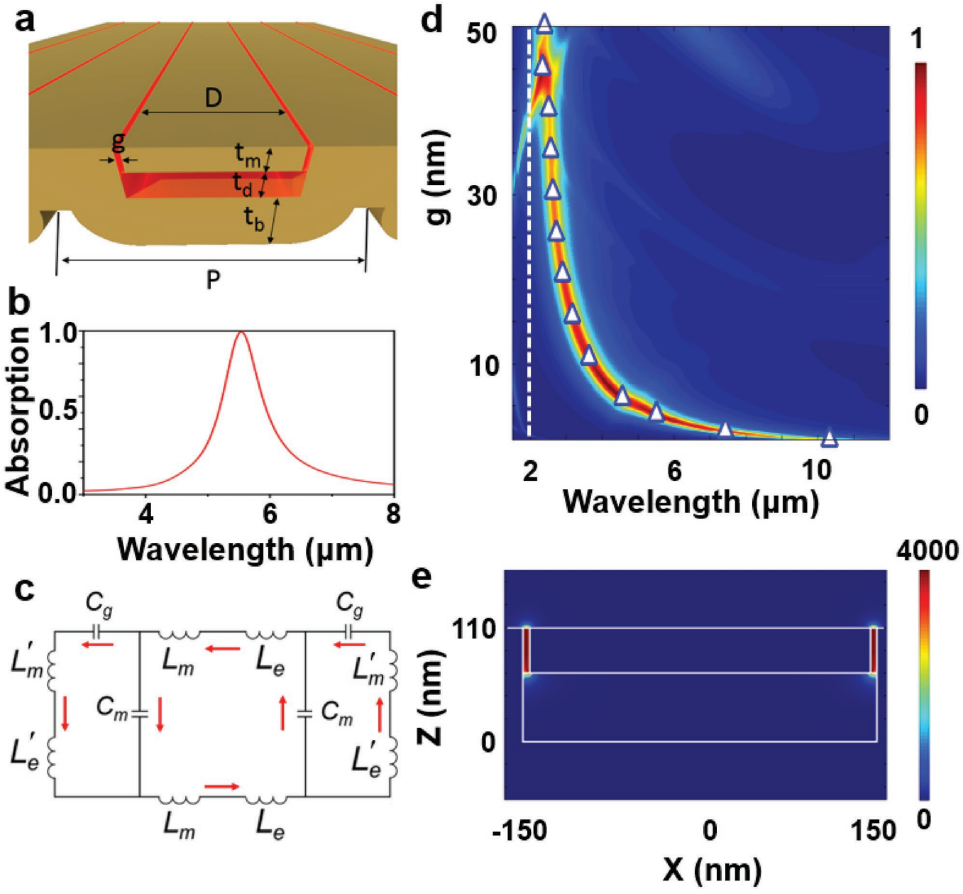


**Figure 2.** a) Schematic illustration of the MDM metamaterial structure with corrugated ground plate. b) Modeled absorption peak of a designed structure with the geometric parameters of ($P$ = 600 nm, $D$ = 300 nm, $t_m$ = 40 nm, $t_d$ = 60 nm, $g$ = 5 nm, $t_b$ = 100 nm). c) Effective circuit model for MDM structure with corrugated ground plate. d) Modeling of the absorption spectra of structure in (a). e) Modeled electric field enhancement distribution around the ultrasmall gap. The peak value of the scale bar is set to 4000 to show the localized field more clearly. The actual peak value is $1.55 \times 10^4$.

wavelength is plotted by empty triangles in Figure 2d, agreeing very well with the numerical modeling results. Due to the significantly increased $C_g$ in the ultrasmall gaps, the resonance will redshift as the gap size decreases. In this case, the light is squeezed into the 5 nm wide gaps leading to a field enhancement factor of $1.55 \times 10^4$ at the resonant wavelength (Figure 2e). Importantly, this corrugated MDM structure with ALD-defined nanogaps is realizable from a fabrication standpoint.

To demonstrate the feasibility, we first deposited an $Ag/Ti/SiO_2$ layer on a glass substrate and then fabricated the periodic patterns with focused ion beam (FIB) milling. The thin Ti film functions as the adhesion layer between Ag and $SiO_2$. Next, this pattern was coated with an ALD-defined ultrathin dielectric film (**Figure 3**a) and another thick Ag film (Figure 3b). Finally, the entire three-layered structure was peeled off to obtain the proposed corrugated super absorber structure (Figure 3c). According to the calibration of our commercial ALD system (Ultratech/Cambridge Nanotech Savannah S100), ≈0.089 nm thick dielectric films can be produced for each cycle reaction under 80 °C, indicating the capability to accurately control the gap size. Following this procudure, a corrugated MDM structure with deep-subwavelength gaps ($P$ = 600 nm, $D$ = 300 nm, $t_m$ = 40 nm, $t_d$ = 60 nm, $g$ = ≈5 nm fabricated by 56 cycles ALD reactions, and $t_b$ = 100 nm) was obtained successfully as shown in Figure 3d (top view) and Figure 3e (cross-sectional view). In this experiment, the FIB milling area is ≈50 μm × 50 μm. Its resonant wavelength is at ≈5.3 μm with the absorption peak of 45% (blue curve in Figure 3f), agreeing well with the numerical modeling based on the extracted geometric parameters (red dots in Figure 3f). Although the geometry of this structure was not optimized yet, the absorption peak is significantly higher than that obtained previously with no super absorber cavity (i.e., 3% as reported in ref. [20]). One can see that the side wall of the metal/$SiO_2$ pattern is not vertical to the substrate plane, demonstrating that one of the major advantages of our corrugated MDM super absorber: i.e., the verticality of the sidewalls of metal patterns and thickness control of second metal layer are no longer critical for fabrication. In addition, this resonant peak can be optimized by suitably designing and fabricating the geometric parameters. For instance, another structure was fabricated successfully (Figure 3g (top view) and Figure 3h (cross-sectional view)) with optimized parameters of $P$ = 500 nm, $D$ = 250 nm, $t_m$ = 30 nm, $t_d$ = 60 nm, $g$ = ≈5 nm, and $t_b$ = 150 nm, realizing a higher absorption peak >81% at the resonant wavelengths of 3.31 μm (blue curve for experimental results and red dots for

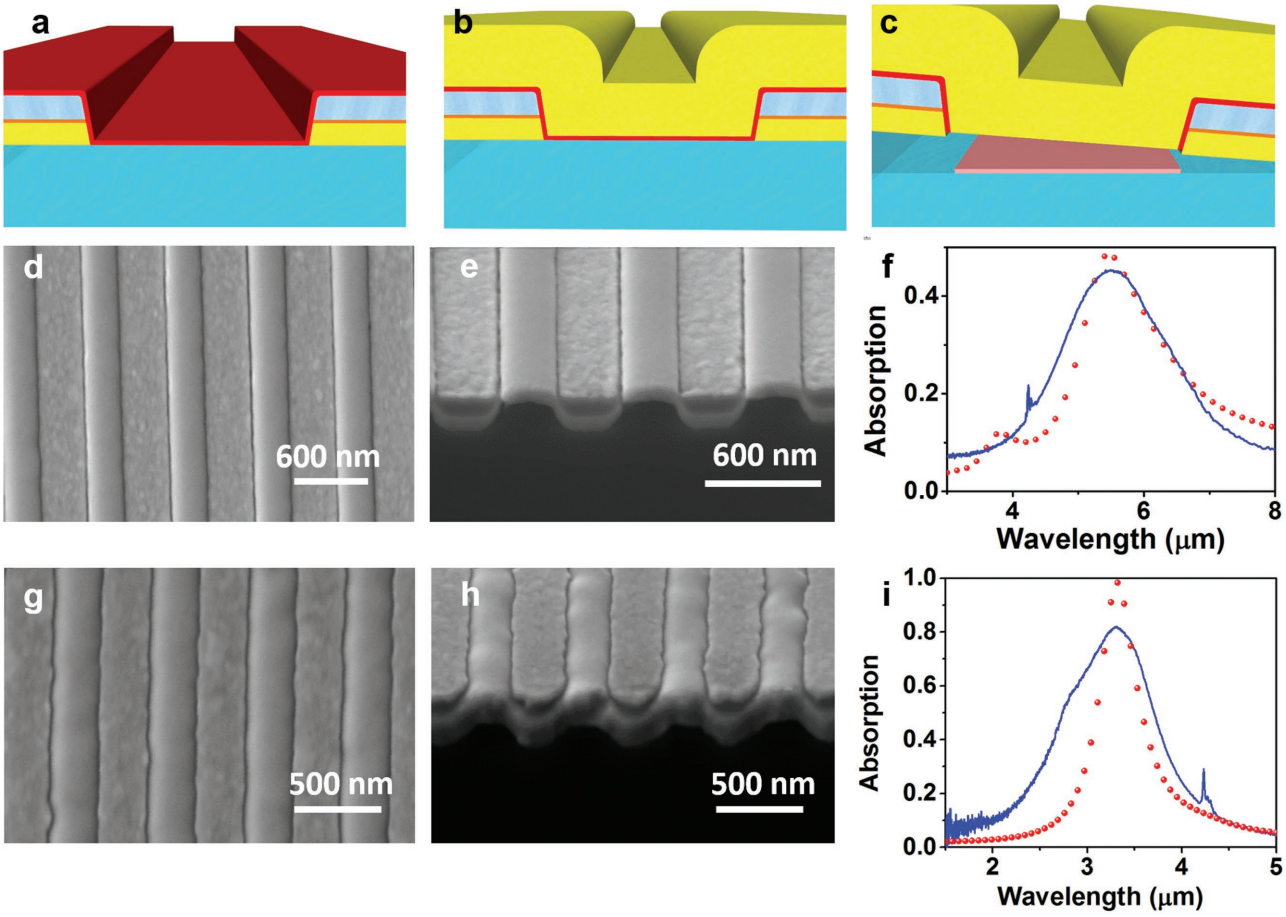


**Figure 3.** a–c) Manufacturing procedure to fabricate corrugated MDM super absorbers with ultranarrow gaps. d) Top-view and e) cross-sectional SEM images of a fabricated structure with the parameter of $P = 600$ nm, $D = 300$ nm, $t_m = 40$ nm, $t_d = 60$ nm, $g = 5$ nm, and $t_b = 100$ nm. f) Measured absorption spectrum of the fabricated structure (blue solid curve) and the modeled absorption curve (red dotted curve) by considering real parameters extracted from the SEM image. g) Top-view and h) cross-sectional SEM images of a structure with the parameter of $P = 500$ nm, $D = 250$ nm, $t_m = 30$ nm, $t_d = 60$ nm, $g = 5$ nm, and $t_b = 150$ nm. i) Measured absorption spectrum of the fabricated structure (blue solid curve) and the modeled absorption curve (red dotted curve) by considering real parameters extracted from the SEM image.

modeling results in Figure 3i). The resonant wavelength can be controlled by tuning the geometry of the nanopatterns. One can refer to Section S1 (Supporting Information) for a design at Terahertz wavelengths. Intriguingly, the dependence of the resonant wavelength on nanogap, as defined by ALD thickness, provides a unique spectral tunability while maintaining fixed lateral dimensions of the first nanopatterns.

## 4. Spectral Tunability with Fixed Lateral Dimensions

In most reported nanophotonic structures (including photonic crystals, plasmonics, and metamaterial structures), period is one of the most important parameters to tune the resonant wavelength. However, for this lateral-dimension-dependent spectral tenability (e.g., Figure 3d–h), advanced top down lithography technologies were mostly required. Even high throughput techniques, such as photolithography and nanoimprint lithography, require different mask/stamp profiles for different lateral dimensions, imposing a significant cost barrier for these types of nanostructure fabrication. Here we will demonstrate a new strategy to realize the spectral tunability based on the same lateral dimension.

As demonstrated in Figures 1b and 2d, due to the strong interaction between adjacent nanopatterns (i.e., the contribution of $C_g$ in Equations (1) and (2)), the resonance can be redshifted using the same lateral dimensions of the metal patterns by using different gap distances defined by ALD processes. To demonstrate this unique spectral tunability, we fabricated a set of three sample with identical lateral dimension, as shown in **Figure 4**a ($P = 300$ nm, $D = 150$ nm, $t_d = 40$ nm, i.e., the first layer pattern illustrated in Figure 3a). On top of these structures, we introduced three different ALD-controlled gaps of 3.03 nm (34 cycles), 4.98 nm (56 cycles), and 7.03 nm (79 cycles), respectively. The ALD film thickness and uniformity was confirmed using a spectral ellipsometer (J. A. Wollam) at nine different areas on the same reference Si substrate coated on the same ALD process. Finally, we deposited the second 200 nm thick metal film to form the complete super absorber structure. One cross-sectional scanning electron microscopy (SEM) image with the gap of ≈5 nm is shown in Figure 4b. As

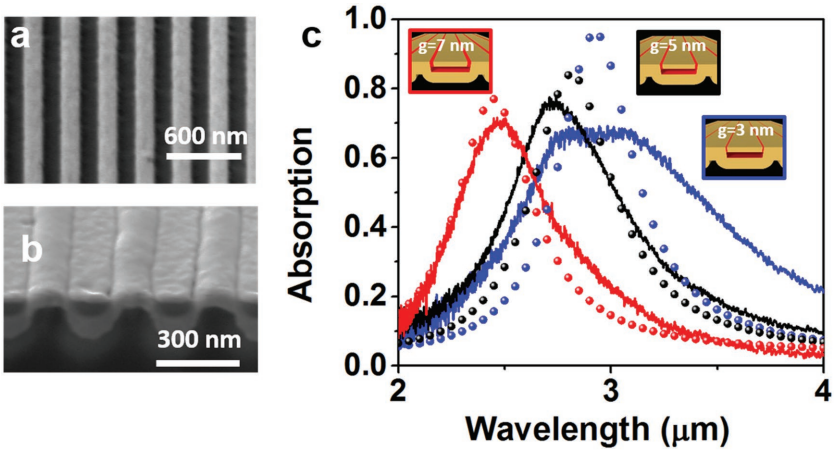


**Figure 4.** a) SEM image of the first layer grating with $P$ = 300 nm and $D$ = 150 nm. b) Cross-sectional SEM image of a fabricated structure ($t_m$ = 40 nm, $t_d$ = 40 nm, and $t_b$ = 200 nm) with the gap size of ≈5 nm. c) Absorption spectra of three samples with different gap sizes of ≈3 nm (blue curve), ≈5 nm (black curve), and ≈7 nm (red curve), respectively. Insets: Schematic illustration of the MDM metamaterial structures with different gaps.

a result, we obtained three different absorption resonance centered at 2.96, 2.74, and 2.48 μm, respectively (solid curves in Figure 4c), agreeing reasonably well with our numerical modeling results (dots in Figure 4c). The relatively large difference in the absorption spectrum for the 3 nm gap sample should be attributed to the fabrication error and intrinsic roughness of the actual structure. These experimental data demonstrated the feasibility of this method for realizing a resonant field enhancement that can be tuned over a wide spectral range with structures that have identical preliminary fabrication steps and patterns (i.e., Figure 3a). To further demonstrate the application of these extremely enhanced localized fields, we will next discuss its application for SEIRA spectroscopy.

## 5. Surface Enhanced Sensing around Ultrasmall Gaps

Infrared (IR) vibrational spectroscopy is one of the most important techniques for chemistry, medicine, and biology, since it can identify molecular composition by analyzing "fingerprints" of signature functional groups.[7,35–38] However, due to the small intrinsic cross-section of a molecular vibration for IR spectroscopy, the sensitivity of this technique is rather limited. In order to obtain vibrational information from extremely small amount of molecules, SEIRA spectroscopy has been developed to improve the detection performance relying on patterned metal surfaces with localized-field enhancement.[35,37–40] Particularly, it is a complementary sensing technique to surface enhanced Raman spectroscopy (SERS): i.e., absorption peaks of SEIRA generally correspond to Raman scattering peaks of SERS. Signals generated by these two technologies could be more sensitive at different spectral regions, complementing each other further. Therefore, an ideal situation is to measure the same sample using these two techniques simultaneously. However, since the vibrational absorption signal of SEIRA is proportional to $|E/E_0|^2$ in contrast to $|E/E_0|^4$ for SERS, the enhancement factor for SEIRA is usually orders of magnitude lower than SERS.[8] This weakness significantly restricts the application of SEIRA in ultrasensitive applications. Recently, various nanopatterns with extremely small gaps were developed to demonstrate enhanced sensitivity for SEIRA applications. For instance, photochemical metal deposition method was employed to fabricate an SEIRA substrate with a 3 nm gap between two nanorod antennas, achieving a signal enhancement over $2 \times 10^5$ experimentally.[38] However, the scalability, uniformity, and reproducibility of nanogaps fabricated by electron beam (e-beam) lithography over small areas remain challenging, something that can be addressed using our proposed corrugated MDM super absorber structure with nanogaps over large areas.[24]

To demonstrate the feasibility, here we employed the structures in Figure 3 as the SEIRA substrates to identify the infrared fingerprints of chemical molecules. When the chemical molecules bind on top of the nanogap and interact with the locally enhanced field (**Figure 5**a), its infrared absorption signal should be enhanced accordingly. In this experiment, we first selected poly(methyl methacrylate) (PMMA) as the sensing target since its absorption finger prints overlap with the absorption band of the fabricated sample in Figure 3d. We spin coated a ≈100 nm thick PMMA layer on our corrugated MDM structure. For comparison, a reference sample was prepared with the same PMMA layer on a flat Ag substrate. Their reflection spectra with and without PMMA coating are plotted in Figure 5b. Since the fabricated 1D structure is polarization dependent, the resonance can only be observed under transverse magnetic (TM) polarized incidence, while under transverse electric polarization, there is negligible structural contribution to the response and the reflection is close to 100%. With TM polarization, a dip at ≈5.5 μm can be observed on the two samples, corresponding to the absorption bands of a carbonyl group (1718.3 $cm^{-1}$) and poly(vinyl acetate) segments (1726.9 $cm^{-1}$) (i.e., signatures of PMMA molecules in SEIRA sensing,[41] indicated by the green dashed lines in Figure 5b,c). One can see that the amplitude of the signal from the MDM structure is obviously stronger than that from the reference sample. For clarity, the difference between the spectra with and without PMMA coating is plotted in Figure 5c, showing that the amplitude of the signature on the MDM structure is enhanced by 11.1. Considering the strongly localized field within the nanogap and the selection rule for SEIRA (i.e., only molecules parallel to the dipole moment of the localized field can be preferentially enhanced),[42] this enhanced signal is actually contributed by a region at the side wall of the first metal pattern that is close to the PMMA-MDM interface. Previously reported works[35,43] generally employed data processing to extract the enhancement factor (see Section S2, Supporting Information, for details). It should be noted that the mid-IR field is strongly localized around the nanogap and decay exponentially away from the interface. Therefore, by analyzing the field distribution obtained by numerical modeling, the

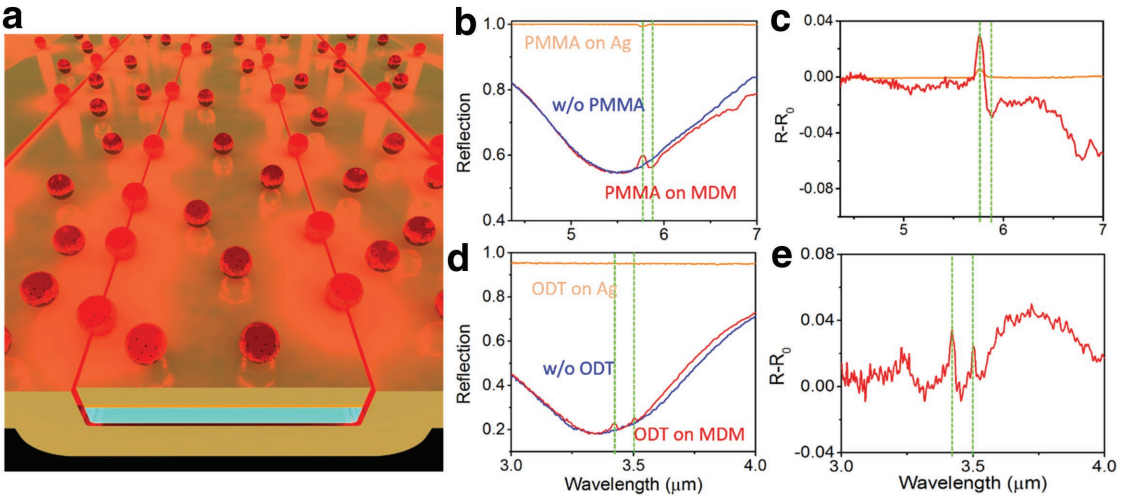


**Figure 5.** a) Conceptual illustration of SEIRA sensing using nanogaps. b) Experimental reflection spectra of nanogap-assisted MDM super absorber with (red curve) and without (blue curve) PMMA coating, and PMMA film directly spin coated on bare Ag film (orange curve). c) Reflection differences for both the nanogap-assisted MDM super absorber sample (red curve) and bare Ag film (blue curve). $R$ and $R_0$ are the reflection of bare Ag film/MDM super absorber with and without PMMA, respectively. d) Experimental reflection spectra of nanogap-assisted MDM super absorber with (red curve) and without (blue curve) ODT coating, and ODT film directly spin coated on bare Ag film (orange curve). e) Reflection differences of nanogap-assisted MDM super absorber sample.

minimum enhancement factor for PMMA layer is estimated from ≈$1.2 \times 10^5$ to $1.8 \times 10^6$, which is two orders of magnitude stronger than the previously reported data for PMMA layers on gold strip grating structures.[44]

To further demonstrate this improved surface enhancement effect, we then coated our sample with a monolayer of 1-octadecanethiol (ODT) molecules to perform the second experiment since their signature fingerprints overlap with the resonance of the structure shown in Figure 3g. According to the ellipsometer characterization, the effective thickness of our sample is ≈2.6 ± 0.2 nm, corresponding to a monolayer ODT molecules.[45] As shown by the orange curve in Figure 5d, the absorption signature signal on the reference Ag sample (i.e., a monolayer of ODT molecules on a flat Ag film) is not resolvable. In contrast, an obvious signal change at 3.42 and 3.5 μm (indicated by the green dashed lines in Figure 5d,e) was observed, corresponding to the signature fingerprints of ODT molecules.[37] The difference between the spectra with and without ODT molecules is plotted in Figure 5e. Since the estimated enhancement factor of SEIRA characterization was dependent on the calculation methods, we then followed two different data processing procedures[20,46] and obtained the enhancement factor of $8.5 \times 10^6$–$1.0 \times 10^7$ (calculation details are listed in Section S3, Supporting Information). This enhancement factor is better than previously reported results based on small area metallic nanorods fabricated by e-beam lithography (e.g., $3.3 \times 10^5$ obtained from a single nanorod with the dimension of 1.4 μm × 100 nm;[46] $1.2 \times 10^5$ obtained from a fan-shaped gold nanoantenna with a ≈20 nm × 20 nm sensing area over a 1.7 μm × 1 μm pattern)[47] and much larger than most reported nanopatterned structures for SEIRA sensing.[37,48] Importantly, the interaction area on top of these nanogaps (e.g., $S_{\text{nanogap}} = 10.6\ \mu m^2$ for the 50 μm × 50 μm structure, see Section S3B, Supporting Information) is much larger than previously reported nanorods (i.e., at the two ends of each rod)[46] and nanoantenna structures (i.e., in the gap area between two metallic tips).[38] Therefore, the signal to noise ratio of our SEIRA result is superior to previously reported results. For instance, for the fan-shaped nanoantenna measured in a similar facility setup as ours,[47] the signal is less than 0.1%, which is ≈40 times smaller than our signal shown in Figure 5e. Due to the weak scattering from the single nanorod,[46] a synchrotron light source was employed to resolve ≈1% signal change. Therefore, a long time scan was required (i.e., taking an average of 125 spectra with 100 scans), ≈60X longer than our measurement. For our current setup, a regular spherical emitter (SiC bar heated at 1300 K) was used as the light source, which provides far less intensity than the synchrotron source and is much more inexpensive and therefore, more accessible for regular sensing applications. As expected, the sensing area can be increased further by reducing the period of the first step patterning while using a smaller gap to obtain the same resonance overlapping with the vibrational mode of molecules (see Section S5, Supporting Information, for an example). More importantly, combined with large area optical interference patterning methods (e.g., 2 cm × 2 cm as we reported in ref. [24] and 10 cm × 10 cm in ref. [49]), the proposed structure is easy to be scaled up over larger areas for the development of inexpensive nanostructured substrates for practical sensing applications. It should be noted that if the ALD-induced $Al_2O_3$ filled in the gap can be removed using etching,[20] more areas/volumes in the gap with strong localized field can be used for extremely enhanced light–matter interaction, which is still under investigation.

In conclusion, we proposed a metamaterial super absorber structure with sub-5 nm gaps. Due to the strong interaction between adjacent patterns, the resonant wavelength can be manipulated by controlling the gap size based on fixed lateral dimensions of major patterns. Using modified ALD processes, a novel metamaterial super absorber structure

with corrugated ground plate was realized. Strong light trapping resonances were obtained in the mid-IR spectral range. Remarkably, these highly efficient trapped light modes are confined within sub-5 nm gaps, resulting in significantly enhanced fields, which are particularly promising for surface enhanced light–matter interaction. According to our experiment demonstration of SEIRA, a sensing enhancement factor over $10^5$–$10^6$ was obtained using PMMA and ODT layers. Due to the large sensing area on top of the nanogaps, the absolute value and signal-to-noise-ratio for SEIRA signal is improved significantly compared with previous reports. This structure is amenble to larger area manufacturing methods like optical interference patterning and nanoimprint lithography. Additionally, the nanogap density (i.e., the sensing area) can be further increased by reducing the basic pattern dimension and the gap size simultaneously. This type of nanogap metamaterial super absorber is particularly attractive for the development of practical nanophotonic platforms for optoelectronic, energy harvesting, conversion and biosensing applications within extreme volumes approaching the plasmonic quantum limit.[13,16,50]

## Supporting Information

Supporting Information is available from the Wiley Online Library or from the author.

## Acknowledgements

D.J. and A.C. contributed equally to this work. Q.G. acknowledges funding support from National Science Foundation (Grant Nos. CMMI1562057 and CBET1445934). S.J. acknowledges funding support from National Science Foundation of China (Grant No. 51572048). N.Z. acknowledges the financial support from Chinese Scholarship Council (CSC).

## Conflict of Interest

The authors declare no conflict of interest.

## Keywords

light confinement, nanofabrication, SEIRA, sub-5 nm gap, superabsorbers

Received: March 8, 2017
Revised: May 7, 2017
Published online:

[1] D. K. Gramotnev, S. I. Bozhevolnyi, *Nat. Photonics* **2014**, *8*, 13.
[2] W. Zhu, R. Esteban, A. G. Borisov, J. J. Baumberg, P. Nordlander, H. J. Lezec, J. Aizpurua, K. B. Crozier, *Nat. Commun.* **2016**, *7*, 11495.
[3] J. A. Schuller, E. S. Barnard, W. Cai, Y. C. Jun, J. S. White, M. L. Brongersma, *Nat. Mater.* **2010**, *9*, 193.
[4] M. Kauranen, A. V. Zayats, *Nat. Photonics* **2012**, *6*, 737.
[5] S. Linic, P. Christopher, D. B. Ingram, *Nat. Mater.* **2011**, *10*, 911.
[6] X. Zhang, Y. L. Chen, R.-S. Liu, D. P. Tsai, *Rep. Prog. Phys.* **2013**, *76*, 046401.
[7] R. Aroca, *Surface-Enhanced Vibrational Spectroscopy*, John Wiley & Sons, Hoboken, NJ **2006**.
[8] P. L. Stiles, J. A. Dieringer, N. C. Shah, R. P. Van Duyne, *Annu. Rev. Anal. Chem.* **2008**, *1*, 601.
[9] H. T. Miyazaki, Y. Kurokawa, *Phys. Rev. Lett.* **2006**, *96*, 097401.
[10] H. T. Miyazaki, Y. Kurokawa, *Appl. Phys. Lett.* **2006**, *89*, 211126.
[11] M. Seo, H. Park, S. Koo, D. Park, J. Kang, O. Suwal, S. Choi, P. Planken, G. Park, N. Park, *Nat. Photonics* **2009**, *3*, 152.
[12] X. Chen, H. R. Park, M. Pelton, X. Piao, N. C. Lindquist, H. Im, Y. J. Kim, J. S. Ahn, K. J. Ahn, N. Park, D. S. Kim, S. H. Oh, *Nat. Commun.* **2013**, *4*, 2361.
[13] K. J. Savage, M. M. Hawkeye, R. Esteban, A. G. Borisov, J. Aizpurua, J. J. Baumberg, *Nature* **2012**, *491*, 574.
[14] R. Esteban, A. G. Borisov, P. Nordlander, J. Aizpurua, *Nat. Commun.* **2012**, *3*, 825.
[15] J. Zuloaga, E. Prodan, P. Nordlander, *Nano Lett.* **2009**, *9*, 887.
[16] M. S. Tame, K. McEnery, Ş. Özdemir, J. Lee, S. Maier, M. Kim, *Nat. Phys.* **2013**, *9*, 329.
[17] Y.-M. Bahk, B. J. Kang, Y. S. Kim, J.-Y. Kim, W. T. Kim, T. Y. Kim, T. Kang, J. Rhie, S. Han, C.-H. Park, *Phys. Rev. Lett.* **2015**, *115*, 125501.
[18] H. Im, K. C. Bantz, N. C. Lindquist, C. L. Haynes, S. H. Oh, *Nano Lett.* **2010**, *10*, 2231.
[19] X. Chen, H.-R. Park, N. C. Lindquist, J. Shaver, M. Pelton, S.-H. Oh, *Sci. Rep.* **2014**, *4*, 6722.
[20] X. Chen, C. Ciraci, D. R. Smith, S. H. Oh, *Nano Lett.* **2015**, *15*, 107.
[21] H.-R. Park, X. Chen, N.-C. Nguyen, J. Peraire, S. H. Oh, *ACS Photonics* **2015**, *2*, 417.
[22] X. Chen, N. C. Lindquist, D. J. Klemme, P. Nagpal, D. J. Norris, S. H. Oh, *Nano Lett.* **2016**, *16*, 7849.
[23] D. Yoo, N.-C. Nguyen, L. Martin-Moreno, D. A. Mohr, S. Carretero-Palacios, J. Shaver, J. Peraire, T. W. Ebbesen, S. H. Oh, *Nano Lett.* **2016**, *16*, 2040.
[24] B. Chen, D. Ji, A. Cheney, N. Zhang, H. Song, X. Zeng, T. Thomay, Q. Gan, A. Cartwright, *Nanotechnology* **2016**, *27*, 374003.
[25] C. M. Watts, X. Liu, W. J. Padilla, *Adv. Mater.* **2012**, *24*, OP98.
[26] N. Liu, M. Mesch, T. Weiss, M. Hentschel, H. Giessen, *Nano Lett.* **2010**, *10*, 2342.
[27] B. Yu, S. Goodman, A. Abdelaziz, D. M. O'Carroll, *Appl. Phys. Lett.* **2012**, *101*, 151106.
[28] A. Moreau, C. Ciraci, J. J. Mock, R. T. Hill, Q. Wang, B. J. Wiley, A. Chilkoti, D. R. Smith, *Nature* **2012**, *492*, 86.
[29] L. Wang, Z. Zhang, *Appl. Phys. Lett.* **2012**, *100*, 063902.
[30] N. Engheta, *Science* **2007**, *317*, 1698.
[31] L. Wang, Z. M. Zhang, *J. Opt. Soc. Am. B* **2010**, *27*, 2595.
[32] L. Fu, H. Schweizer, H. Guo, N. Liu, H. Giessen, *Phys. Rev. B* **2008**, *78*, 115110.
[33] J. Zhou, E. N. Economon, T. Koschny, C. M. Soukoulis, *Opt. Lett.* **2006**, *31*, 3620.
[34] N. Van Der Meijs, J. Fokkema, *Integration* **1984**, *2*, 85.
[35] R. Adato, A. A. Yanik, J. J. Amsden, D. L. Kaplan, F. G. Omenetto, M. K. Hong, S. Erramilli, H. Altug, *Proc. Natl. Acad. Sci. USA* **2009**, *106*, 19227.
[36] Y. Li, L. Su, C. Shou, C. Yu, J. Deng, Y. Fang, *Sci. Rep.* **2013**, *3*, 2865.
[37] L. V. Brown, K. Zhao, N. King, H. Sobhani, P. Nordlander, N. J. Halas, *J. Am. Chem. Soc.* **2013**, *135*, 3688.
[38] C. Huck, F. Neubrech, J. Vogt, A. Toma, D. Gerbert, J. Katzmann, T. Härtling, A. Pucci, *ACS Nano* **2014**, *8*, 4908.
[39] D. Dregely, F. Neubrech, H. Duan, R. Vogelgesang, H. Giessen, *Nat. Commun.* **2013**, *4*, 2237.
[40] S. Lal, N. K. Grady, J. Kundu, C. S. Levin, J. B. Lassiter, N. J. Halas, *Chem. Soc. Rev.* **2008**, *37*, 898.
[41] R. Ahmed, *Int. J. Polym. Mater.* **2008**, *57*, 969.

[42] M. Osawa, *Top. Appl. Phys.* **2001**, *81*, 163.
[43] S. Aksu, A. E. Cetin, R. Adato, H. Altug, *Adv. Opt. Mater.* **2013**, *1*, 798.
[44] T. Wang, V. H. Nguyen, A. Buchenauer, U. Schnakenberg, T. Taubner, *Opt. Express* **2013**, *21*, 9005.
[45] M. J. Tarlov, *Langmuir* **1992**, *8*, 80.
[46] F. Neubrech, A. Pucci, T. W. Cornelius, S. Karim, A. García-Etxarri, J. Aizpurua, *Phys. Rev. Lett.* **2008**, *101*, 157403.
[47] L. V. Brown, X. Yang, K. Zhao, B. Y. Zheng, P. Nordlander, N. J. Halas, *Nano Lett.* **2015**, *15*, 1272.
[48] W.-C. Shih, G. M. Santos, F. Zhao, O. Zenasni, M. M. P. Arnob, *Nano Lett.* **2016**, *16*, 4641.
[49] T. Siegfried, Y. Ekinci, H. Solak, O. J. Martin, H. Sigg, *Appl. Phys. Lett.* **2011**, *99*, 263302.
[50] C. Ciracì, R. Hill, J. Mock, Y. Urzhumov, A. Fernández-Domínguez, S. Maier, J. Pendry, A. Chilkoti, D. Smith, *Science* **2012**, *337*, 1072.

 